Journal of the Meteorological Society of Japan, Vol. 94, No. 5, pp. 443−452, 2016
DOI:10.2151/jmsj.2016-022

NOTES AND CORRESPONDENCE

A Grid Transformation Method for a Quasi-Uniform, Circular Fine Region Using the Spring Dynamics

Ryosuke SHIBUYA, Hiroaki MIURA, and Kaoru SATO

Department of Earth and Planetary Science, The University of Tokyo, Tokyo, Japan

(Manuscript received 10 December 2015, in final form 25 May 2016)

Abstract

Regionally enhanced meshes that have quasi-uniformly fine circular region is proposed using a new transformation method with icosahedral grids to obtain a cost-effective simulation for waves, transports, and mixing processes, the behaviors of which depend strongly on the horizontal resolution. The target region, which is designed to be composed of a finer mesh, is connected to a coarser mesh region, which is generated with the Schmidt transformation to maintain an isotropy of grid shapes. To realize these requirements, the spring dynamics method can be used and the characteristic length of the spring connecting grid nodes should be determined through three parameters: (i) the number of grid points placed in the target region, (ii) the area of the target region, and (iii) a parameter of the Schmidt transformation. By introducing a set of mathematical formulae, the minimum grid interval in the target region can be uniquely determined as a function of the area of the target region only. It is confirmed that fine and quasi-homogeneous meshes in the target region are generated using the grid transformation proposed in this study. Numerical simulations under realistic atmospheric conditions are performed using a non-hydrostatic model with the grid system proposed in this study and in a previous study. As the new grid system has a more homogenous resolution in the target region compared with that of the previous study, the estimation of the momentum fluxes of gravity waves are less affected by their dependence of the grid resolution.

Keywords icosahedral grid; stretched grid; spring dynamics; numerical model

1. Introduction

The rapid development of computational facilities has allowed the horizontal resolution of atmospheric general circulation models to be sufficiently fine to resolve non-hydrostatic scale motions. In such high-resolution models, the discretization of a system of equations using grid-point methods on polyhedral grids seems to be preferred because of its high computational performance on parallel computers. An icosahedral grid is such a choice (e.g., Williamson 1968; Sadourny et al. 1968; Heikes and Randall 1995). The Non-hydrostatic ICosahedral Atmospheric Model (NICAM) is an example of such a model that uses icosahedral grids, albeit with some modifications (Tomita et al. 2002). Detailed descriptions of the dynamical core and recent developments of NICAM are given by Tomita and Satoh (2004), Satoh et al. (2008), and Satoh et al. (2014). Recently, Miyakawa et al. (2014) showed that NICAM performed well in predicting Madden–Julian Oscillation (MJO) for nearly one month. The icosahedral grids have been perceived to be useful based on those demonstrations using high-resolution simulations.

Corresponding author: Ryosuke Shibuya, The University of Tokyo, 7-3-1 Hongo, Bunkyo-ku, Tokyo 113-0033, Japan
E-mail: shibuya@eps.s.u-tokyo.ac.jp
J-stage Advance Published Date: 10 June 2016

If computational resources are limited, however, we cannot use fine and uniform horizontal meshes over the globe and generating finer meshes about a targeted region may be a better choice. In such a case, regional or nesting models are commonly chosen to reduce computational burden. However, regional or nesting models can suffer from serious issues due to the existence of artificial boundaries. Because boundary conditions are inevitably needed in these models, some technical treatments are required regarding the boundary to reduce numerical errors or to damp artificial reflections of waves. These problems can be avoided using the stretched grid transformation developed by Tomita (2008). He constituted a transformation function based on the Schmidt transformation function and applied it to the icosahedral grids. His transformation allows us to gather grid points into a local region of interest and realize higher resolution near the point. Because the resolution changes smoothly away from the central point of the local region of interest, no lateral boundary condition is required in its grid transformation. This is an obvious advantage of this approach. This type of smooth transition is useful, especially for case studies that require high resolution in a limited region for a sufficiently short period. For example, the stretched grid is used to examine the prediction skill of MJO during the CINDY2011/DYNAMO observation period (Nasuno et al. 2013) and to simulate the dynamics of multiple tropopause events and inertia–gravity waves in the Antarctic (Shibuya et al. 2015).

However, one should be cautious when the stretched grid made by Tomita (2008) is applied to analyze phenomena whose expressions strongly depend on the horizontal resolution. This is due to the fact that the stretched grid does not maintain a constant cell interval in the high-resolution region where we want to focus (hereafter, we refer to this region as "the target region"). This feature becomes apparent when the stretching parameter, the definition of which will be given below, is large. Such a non-negligible resolution change over the target region likely causes problem associated with the spatial dependence of the simulation results. For example, Plougonven et al. (2013) compared two simulations with different resolutions and reported that when the horizontal resolution is doubled, the amplitudes of inertia–gravity waves become almost twice as large, although the phase structures of the waves do not greatly differ in either resolution. Aghedo et al. (2010) shows that the passive tracer transports in the ECHAM5 general circulation model strongly depend on the horizontal and vertical resolutions. Because the horizontal resolution inherently determines the finest scale of the filament around the barrier regions, such as the tropopause and edge of the polar vortex, the mixing processes resolved in the numerical model have a strong dependence on the grid resolution. Therefore, to examine physical processes such as waves, transports, and mixing processes with limited computational resources, quasi-uniform and regionally finer meshes around the targeted region are desirable.

Iga (2015) proposed a smooth and seamless grid system with several topologies based on a conformal mapping technique. This grid system has a fine and uniform resolution inside the target region and is applicable to both the equatorial and polar regions. However, this new method is implemented with the polyhedral grids, which is different from an icosahedral one. In the current study, we intended to maintain the icosahedral grid structure and to develop another approach to configure a grid system with fine and quasi-homogeneous resolution in the target region. The finer mesh region is connected to the coarser mesh region transformed by the Schmidt transformation. The grid system is modified by the spring dynamics method (Tomita et al. 2002), but we modify the characteristic length of the spring connecting grid nodes depending on the location of the spring. Moreover, we formulate a constraint between the horizontal resolutions, an area of the target region, and the total number of points in the mesh; the finest possible resolution inside the target region can be specified by an analytical function of an area of the target region.

The structure of this article is as follows. A method of a standard grid generation in NICAM is reviewed in Section 2, since we apply the basic grid generation method in NICAM to a new grid formation proposed in this study. In Section 3, we derive a mathematical constraint of the characteristic spring length in the variable-resolution grid system regarding the connection with the Schmidt transformation. The results of the new transformation are compared with those of the method by Tomita (2008) in Section 4. The spatial structures of grid properties, such as the isotropy and the smoothness, are also analyzed. Section 5 summarizes the results and gives concluding remarks.

2. A standard grid generation method in NICAM

2.1 Icosahedral grid on a sphere

Icosahedral grids over the sphere are generated by recursively dividing the original icosahedron. In NICAM, the grid resolution generated by the n-th

dividing operation is conventionally referred to as the "glevel-n" (grid division level n) grid (Tomita et al. 2002). Glevel-0 is the original icosahedron. By dividing each triangle into four small triangles, a higher-level mesh is obtained. The total number of node points is $N = 10 \cdot 4^n + 2$ for glevel-n. The effective resolution is estimated by the square root of the averaged control volume area, $\sqrt{4\pi R_E^2 / N}$, where R_E is the Earth's radius. Throughout the rest of the paper, the unit sphere is assumed. It should be noted that the grid can simply be scaled to whatever radius sphere is needed by the model.

2.2 Spring dynamics

In NICAM, grid intervals are regularized by the spring dynamics method and are re-modified by the gravitational-centered relocation (Tomita et al. 2002), which guarantees the second-order accuracy of numerical differential operators in NICAM (Tomita et al. 2001). It is assumed that each grid point has its own mass M and that neighboring grid points are connected by a spring with the spring coefficient k and the characteristic length f. A damping force proportional to the velocity of the grid motion is also added to ensure that the system calms down to a quasi-steady state after a sufficient number of iterations. The equation of the grid point motion is described as

$$M\frac{d\vec{w_0}}{dt} = \sum_{i=1}^{n} k(d_i - f)\vec{e_i} - \alpha\vec{w_0}, \quad \text{and} \quad \frac{d\vec{r_0}}{dt} = \vec{w_0}, \tag{1}$$

where d_i is the distance between the point P_0 and P_i, where P_i is one of grid points surrounding P_0, $\vec{e_i}$ is the unit vector in the direction from P_0 to P_i projected on the tangential plane at P_0, $\vec{w_0}$ is the velocity vector at P_0, $\vec{r_0}$ is the position vector of P_0, n is the number of mass points surrounding P_0, and α is a damping coefficient. When the grid system reaches the equilibrium state, the following relation is satisfied:

$$\sum_{i=1}^{n}(d_i - f)\vec{e_i} = 0, \tag{2}$$

because $d\vec{w_0}/dt = 0$ and $\vec{w_0} = 0$.

An initial location of grid points before the iterations of the spring dynamics should be carefully prepared to avoid the collapse of grid shapes. One of the technical ways to prepare the initial grid location is as follows: First, the grid transformation with a low g-level (2 or 3) is conducted with the initial condition of the original icosahedron. The grid configuration in higher g-level can be sequentially generated with the initial grid location of the same grid configuration with the lower g-level by making a new grid point at the midpoint of the grid point in the lower-glevel.

The grid structure in the equilibrium state depends only on a constant characteristic length f. In this study, we add a dependence on latitude to ϕ to f, that is, $f(\phi)$, to enable the variable-resolution system. This also means that we expect the spring dynamics to force the distance between two grid points to be close to the latitude-dependent characteristic length $f(\phi)$. The specific form of the function $f(\phi)$ is discussed in Section 3.

3. How to determine characteristic spring length

3.1 A constraint on a cell area and a total grid number over the sphere

Let us generate a local region constituted of a quasi-homogeneous grid (i.e., a target region). In particular, we focus on the region around the North Pole and try to generate the target region with a fine and quasi-homogeneous grid. In this case, the perimeter of the target region is just along a latitude ϕ_0. When an effective resolution is defined as the square root of a cell area, the effective resolution of a cell in the target region dx_T is determined by the area of the target region and the number of cells n in the target region because the grids in the target region are designed to be quasi-uniform. Thus, dx_T is given by

$$dx_T = \sqrt{\frac{2\pi\,(1-\sin\phi_0)}{n}}. \tag{3}$$

Hereafter, we refer to this latitude ϕ_0 as the edge latitude. As discussed in Section 2.1, the unit sphere is assumed.

Outside the target region, the resolution is modified by determining a latitude-dependent length scale $f(\phi)$, that is used by the spring dynamics method as a characteristic length scale of the spring. Assuming a regular hexagon, the area of the cell is equal to $\sqrt{3}/2(f(\phi))^2$ (see Fig. 1 in Tomita et al. 2002). Hereafter we refer $f(\phi)$ as "the grid interval function." Note that $f(\phi)$ is an arbitrary function that takes positive values for $-\pi/2 \le \phi \le \pi/2$.

An obvious constraint on the cell areas over the sphere is that the integration of all cell areas must be equal to the area of the sphere. This constraint can be written as follows:

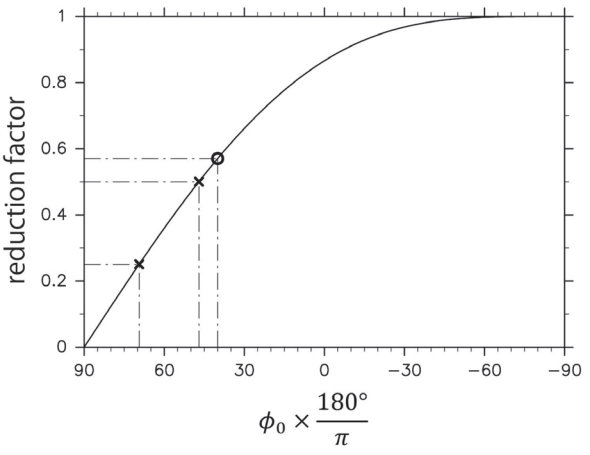

Fig. 1. The reduction ratio as a function of the edge latitude ϕ_0. The cross-marks denote the points at which the reduction ratios are 0.5 and 0.25. The circle denotes the point at $\phi_0 = 40°\pi/180°$.

$$\int_0^{2\pi}\int_{-\pi/2}^{\pi/2}\frac{\cos\phi}{A(\phi)}d\phi d\lambda = N,$$

where λ is longitude, ϕ is latitude, N is the number of grid points over the sphere, and $A(\phi)$ is a cell area around a grid point (λ, ϕ).

If the number of cells, n is specified in the target region, the grid interval function, $f(\phi)$, which is outside the target region,must satisfy the following equation

$$2\pi\int_{-\pi/2}^{\phi_0}\frac{\cos\phi}{\frac{\sqrt{3}}{2}(f(\phi))^2}d\phi = N - n. \tag{4a}$$

Additionally, to enforce a smooth connection between the target region ($\phi_0 \le \phi \le \pi/2$) and the remaining outer region ($-\pi/2 \le \phi \le \phi_0$), the resolution at ϕ_0 should be equal to dx_T. These conditions are written as

$$\sqrt{\frac{2\pi(1-\sin\phi_0)}{n}} = \sqrt{\frac{\sqrt{3}}{2}}f(\phi_0). \tag{4b}$$

Although $f(\phi)$ is an arbitrary function that satisfies Eqs. (4a) and (4b) at this point, it is obviously desirable if $f(\phi)$ is chosen so that the quasi-isotropy of a grid system can be realized. A form of such $f(\phi)$ will be given in the next section.

3.2 Connection with the Schmidt transformation

As verified by Tomita (2008), the transformation that can maintain the isotropy of the grid is identical to a Schmidt transformation. This isotropic transformation is introduced by

$$\phi = \sin^{-1}\left[\frac{\beta(1+\sin\Phi)/(1-\sin\Phi)-1}{\beta(1+\sin\Phi)/(1-\sin\Phi)+1}\right], \tag{5}$$

where Φ is the latitude of the original point before the transformation, ϕ is the latitude after the transformation, and β is the stretching parameter that enables the smooth transition of the horizontal resolution. The latitudinal change of the latitude interval by the transformation, $d\phi/d\Phi$ can be interpreted as the reduction factor of the grid interval, and the resolution after the transformation, $G(\Phi)$, is analytically derived as

$$G(\Phi) = dx\frac{d\phi}{d\Phi} = dx\frac{2\sqrt{\beta}}{(\beta+1)+(\beta-1)\sin\Phi}, \tag{6}$$

where dx is the grid interval before the transformation. It should be noted that Eq. (6) indicates the resolution as a function of the original latitude Φ. For example, $G(\Phi)|_{\Phi=0}$ gives the resolution not at the equator, but at the latitude to which the equatorial line is transformed, i.e., $\sin^{-1}\left[\frac{\beta-1}{\beta+1}\right]$. The inverse of the Schmidt transform is given by

$$\Phi = \sin^{-1}\left[\frac{-(\beta+1)\sin\phi+(\beta-1)}{(\beta-1)\sin\phi-(\beta+1)}\right] \equiv S^{-1}(\phi). \tag{7}$$

Thus, the resolution is derived as a function of the transformed latitude ϕ using Eq. (7),

$$G(S^{-1}(\phi)) = dx\frac{(\beta+1)-(\beta-1)\sin\phi}{2\sqrt{\beta}}. \tag{8}$$

It is easily verified by substituting $\phi = \pi/2$ into Eq. (8) that the grid resolution is changed by a factor of $1/\sqrt{\beta}$ at the center of the transformation. When $\beta > 1$, the refinement for $\phi > 0$ in the northern hemisphere is obtained, while $0 < \beta < 1$ makes the refinement for $\phi < 0$ in the southern hemisphere.

We use the Schmidt transformation as the grid interval function to obtain an isotropic grid structure outside of the target region. This Schmidt transformation has the same number of grid points outside the target region, $N - n$, as our new transformation. In the target region, however, this Schmidt transformation needs a larger number of grid points, n', than the number of grid points used in our new transfor-

mation, n. This is because the grid intervals obtained by the Schmidt transformation in the target region are smaller than the designed transformation Thus an original grid resolution used the Schmidt transformation, $dX = \sqrt{4\pi / (n' + (N - n))}$, is different from the quasi-homogeneous grid interval, $dx = \sqrt{4\pi / (n + (N - n))}$. Therefore, the grid interval function outside the target region is obtained as follows:

$$\sqrt{\frac{\sqrt{3}}{2}} f(\phi) = dX \frac{(\beta+1) - (\beta-1)\sin\phi}{2\sqrt{\beta}}, \quad -\pi/2 \le \phi \le \phi_0. \tag{9}$$

Recall that at ϕ_0, the resolution in the target region is equal to the resolution after the Schmidt transform. We can, therefore, determine dX by combining Eqs. (4b) and (9) and arrive at the grid interval function that generates quasi-uniform grids in the target region and connected to the Schmidt transformation is obtained:

$$f(\phi) = \begin{cases} \sqrt{\frac{2}{\sqrt{3}}} \sqrt{\frac{2\pi(1-\sin\phi_0)}{n}}, & \phi_0 \le \phi \le \pi/2 \\ \sqrt{\frac{2}{\sqrt{3}}} \sqrt{\frac{2\pi(1-\sin\phi_0)}{n}} \frac{(\beta+1) - (\beta-1)\sin\phi}{(\beta+1) - (\beta-1)\sin\phi_0}, & -\pi/2 \le \phi \le \phi_0. \end{cases} \tag{10}$$

Three parameters of the transformation, β, n, and ϕ_0 in Eq. (10) are related through the constraint about the grid system over the sphere, Eq. (4a).

3.3 *The mathematical constraints on ϕ_0, n, and β*

Using $f(\phi)$ as defined by Eqs. (10) and (4a), we obtain a single equation about three unknowns, ϕ_0, n and β:

$$n \frac{((\beta+1) - (\beta-1)\sin\phi_0)^2}{1-\sin\phi_0} \int_{-\pi/2}^{\phi_0} \frac{\cos\phi}{((\beta+1) - (\beta-1)\sin\phi)^2} d\phi = N - n. \tag{11}$$

Equation (11) relates three parameters of the transformation, β, n, and ϕ_0. Here, we can ask a following question: for a given value of ϕ_0, what is the largest number of cells, n, that the transformation can place in the target region subject to the constraint that β be a positive, real value? We can transform Eq. (11) into a function of β and ϕ_0 that gives the number of cells in the target region:

$$n(\phi_0, \beta) = N \left[\int_{-\pi/2}^{\phi_0} \frac{((\beta+1) - (\beta-1)\sin\phi_0)^2 \cos\phi}{(1-\sin\phi_0)((\beta+1) - (\beta-1)\sin\phi)^2} d\phi + 1 \right]^{-1}. \tag{12}$$

For a fixed ϕ_0, $n(\phi_0, \beta)$ monotonically increases with increasing β. Using this fact, we can, therefore, place an upper bound on the number of cells in the target region by taking the limit as $\beta \to \infty$:

$$n_{\lim} = \lim_{\beta \to \infty} n(\phi_0, \beta) = \frac{2N}{3 + \sin\phi_0}. \tag{13}$$

Thus, $n_{\lim}$ is an upper bound on n:

$$n < \frac{2N}{3 + \sin\phi_0} = n_{\lim}. \tag{14}$$

This condition also indicates that the minimal resolution in the target region is also bounded by

$$dx_T = \sqrt{\frac{2\pi(1-\sin\phi_0)}{n}} > \sqrt{\frac{2\pi(1-\sin\phi_0)}{n_{\lim}}}. \tag{15}$$

Substituting the definition of $n_{\lim}$ from Eq. (14) into Eq. (15), we obtain

$$dx_T > \sqrt{\frac{4\pi}{N}} \sqrt{\frac{3 - 2\sin\phi_0 - \sin^2\phi_0}{4}} = dx_{T_{\min}}. \tag{16}$$

This inequality indicates that the minimal resolution $dx_{T_{\min}}$ is proportional to the original resolution $\sqrt{4\pi / N}$ multiplied by the reduction factor $\sqrt{(3 - 2\sin\phi_0 - \sin^2\phi_0)/4}$. Figure 1 shows the reduction factor as a function of the edge latitude ϕ_0. The reduction factor is one for $\phi_0 = -\pi/2$, corresponding to the original grid shape and is zero for $\phi_0 = \pi/2$, corresponding to the case where all grid points are located at the pole. When we set ϕ_0 as $\sin^{-1}(-1 + \sqrt{3})$ approximately 47°) or $\sin^{-1}(-1 + \sqrt{15/4})$ (approximately 69.5°), the reduction factor becomes 0.5 or 0.25, respectively. This corresponds to the increase by one or two g-levels in the target region.

For a given ϕ_0, a sufficiently large value of β is needed so that the number of the grid points in the target region, n, approaches $n_{\lim}$ (Eq. 13). However, a typical value of β at which $dn/d\beta$ is close to zero is dependent on the choice of ϕ_0 (not shown). Thus, in practice, it is better to choose the largest integer less than $0.99 \times n_{\lim}$ as n, which gives $\sqrt{1/0.99}$ (~1.005) $dx_{T_{\min}}$ in the target region. Finally, after the dependent

parameter β is numerically solved through Eq. (11), we obtain an ideal variable-resolution grid system using Eq. (10).

Note again that the quasi-homogeneous grid system in the target region is obtained using only one parameter, ϕ_0 through Eqs. (11) and (13). The meaning of the parameter ϕ_0 is clear: it is the edge latitude of the target region.

4. Results: Grid properties

We use the grid interval function given by (10) as the characteristic length in the spring dynamics in Section 2.2. Hereafter, we select $\phi_0 = 40°$. In that case, $n = 0.99 \times n_{\rm lim} \sim 0.99 \times 0.55N$ and $\beta \sim 205.3$. In this section, the g-level of the grid system is 7 ($\sim 4^{\rm glevel} \times 10$ grid points).

The stretched grid transformed by the original method of Tomita (2008) is also generated with the same number of grid points in the target region for the comparison. The stretching parameter β in Tomita (2008) is approximately $\beta = 5.42$. After relocating the grid points near the North Pole using both transformation, we rotate all grids such that the center of the target region is located at the South Pole. This is because we present results of the simulations in Section 4.3, which focus on gravity waves around the Antarctic. It should be noted that, in Schmidt transformation, the transformation after the relocation to the South Pole just corresponds to the Schmidt transformation using $\beta = 5.42^{-1}$.

4.1 Resolution

Figure 2 shows a scatter plot of the normalized grid intervals, defined as $d \times 2^{\rm glevel}$ (d denotes the grid interval), at all grid cells as a function of the latitude. The result of our transformation (green cross marks) seems similar to the input characteristic length (Eq. 9) (a black solid curve), although some discrepancies around pentagonal cells appears. This may be partly explained by the properties of the spring dynamics, which leads to smaller grid intervals around pentagons (as discussed in Tomita et al. 2002).

Figure 3 shows the horizontal map of the ratio of the normalized grid intervals. The grid intervals in Fig. 3 are averaged between the point P_0 and surrounding points. Compared with the transformation in Tomita (2008), it is clear that the grid intervals in the target region are more homogeneous and coarse in the non-target region. It should be noted that this feature is preferable to reduce the computational burden, since our transformation does not require the model to use a smaller time step due to the existence of a few small cells.

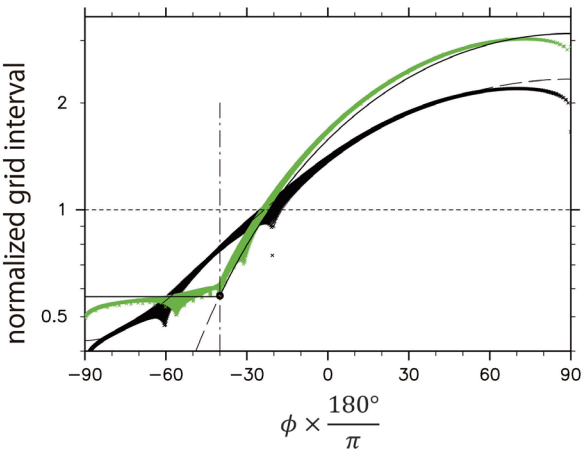

Fig. 2. The scater plots of the normalized grid interval defined as $d \times 2^{\rm glevel}$ (d denotes the grid interval) as a function of the latitude in the result of our transformation (green cross marks), the Schmidt transformation with $\beta = 5.42$ (black cross marks), the input characteristic length (black solid line), and the theoretical grid interval of the transformation by Tomita (2008) (black dashed curve). The g-level is 7 ($\sim 4^{\rm glevel} \times 10$ grid points). The black circle and dot-and-dashed line at $\phi_0 = 40°$ denote the connection point to the Schmidt transformation.

4.2 Smoothness and Isotropy

Next, we examine and compare the grid properties, such as area uniformity and isotropy, in both grid systems. The area uniformity is important to resolve some dynamical phenomena, such as waves and mixing processes, as discussed in Section 1. In this study, the area uniformity is locally defined by the variance of a grid area against areas of the surrounding grids as a measure of smoothness:

$$S_0 = \frac{\sum_{i=1}^{N_s} (A_i - A_0)^2}{N_s A_0^2}, \tag{17}$$

where A_0 is an area of a grid, A_i is that of a grid surrounding A_0, and N_s is the number of grids surrounding A_0. When the grid areas are completely smooth, the area uniformity S_0 is zero. It should be noted that S_0 is normalized by the square of its own grid area to ignore the effect of the g-level because the variance of the area $\sum_{i=1}^{N_s} (A_i - A_0)^2$ depends on the grid area itself in the same configuration.

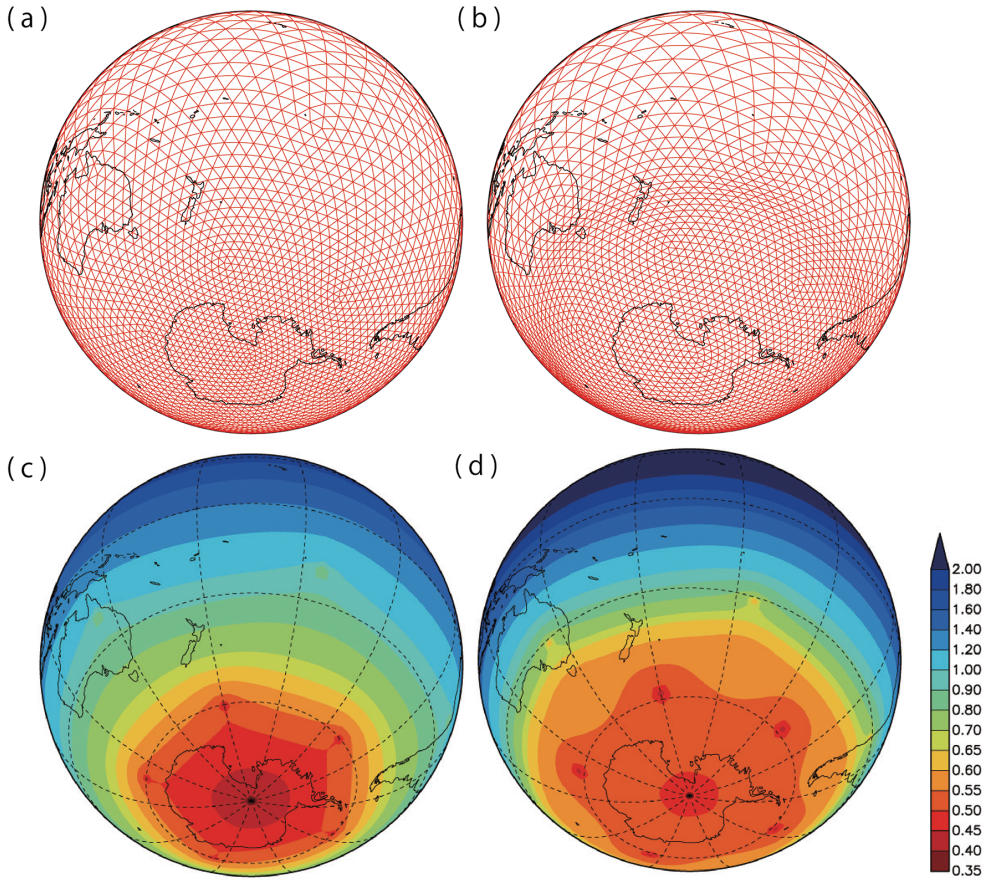

Fig. 3. The stretched icosahedral grid by (a) the transformation with $\beta \sim 5.42$ in Tomita (2008) and (b) the present transformation. The horizontal map of the normalized grid interval (c) with the same grid as (a), and (d) with the same grid as (b). The g-level is 7 in (c) and (d), while it is degraded from g-level 7 to 4 in (a) and (b) for simplicity.

Figure 4a shows the area uniformity S_0 in the transformation by Tomita (2008) and the present transformation. It is clear that the distribution of the grid areas is smoother in the target region in our transformation than Tomita (2008) although the smoothness of our transformation is larger outside the target region. The local maxima at the pentagonal grids exist in both transformations.

The isotropy is also an important component for grid configuration because the break of the isotropy causes the dependence of minimal resolvable scales on axis directions (Miura and Kimoto 2005). Miura and Kimoto (2005) defined the isotropy of the icosahedral grid as

$$I_0 = \frac{\sum_{i=1}^{N_s} (l_i - l_0)^2}{N_s l_0^2}, \qquad l_0 = \frac{\sum_{i=1}^{N_s} l_i}{N_s}, \tag{18}$$

where l_i is one edge length of a cell and l_0 is the mean edge length of a cell. When the grid shapes are completely isotropic, the isotropy I_0 is zero.

Since the transformation by Tomita (2008) is based on the Schmidt transformation, which is one of theoretical isotropic transformations, we will regard the isotropy of the meshes by Tomita (2008) as the reference of an isotropic transformation.

Figure 4b shows a scatter plot of the isotropy I_0 of the grid shapes in the transformation by Tomita

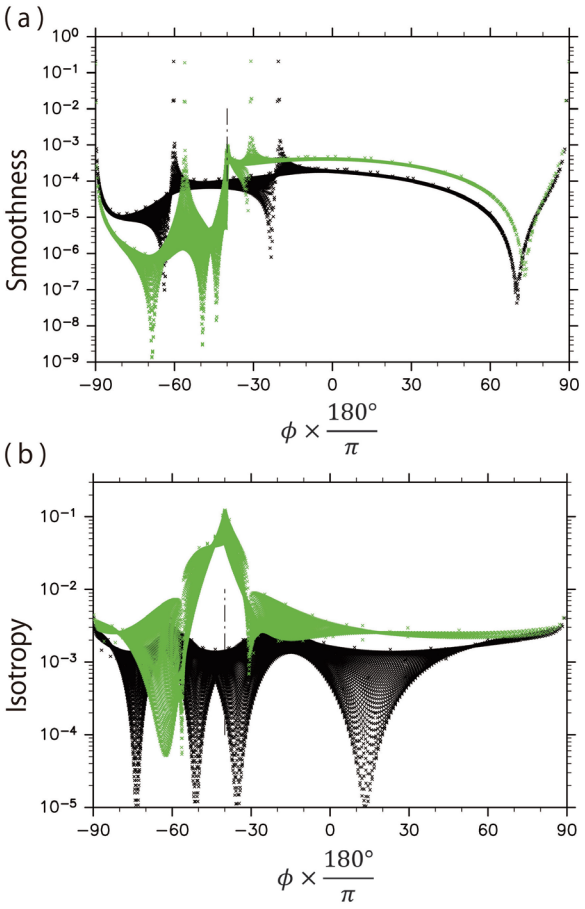

Fig. 4. The scatter plots of the (a) smoothness and (b) isotropy at all grids as a function of the latitude in the present transformation (green cross marks) and the transformation in Tomita (2008) (black cross marks). The g-level is 7 (~ 4^{glevel} × 10 grid points).

(2008) and the present transformation. The isotropy in our transformation has large maxima around the edge latitude $\phi_0 = -40°$, compared with that in Tomita (2008). The distortion of the grid shape around the edge latitude can be also found in Fig. 3b. In Fig. 4b, such disfftorted cells are located inside the target region with the width of about 15° from the edge latitude. This fact may suggest that the target region should be designed broader than the region on which we want to focus on. At other latitudes, the value of I_0 in our transformation is approximately 3.0×10^{-3}, while the value of I_0 in Tomita (2008) is about 1.5×10^{-3}. Because $\sqrt{I_0}$ means a ratio of a standard deviation of edge lengths of a cell to the mean edge length, a cell with $I_0 = 3.0 \times 10^{-3}$ (1.5×10^{-3}) has surrounding edge lengths with the standard deviation of approximately 5.5 % (3.9 %) of the mean edge length. Thus, by our transformations, the meshes show almost isotropic grid shapes, except the edge latitude.

4.3 *Numerical simulation*

In this subsection, pairs of simulations are conducted for a realistic atmospheric condition using NICAM with two grid systems. One is generated by our transformation and the others by the transformation of Tomita (2008), as shown in Figs. 3a and 3b, respectively. The initial condition and model configuration, except the horizontal grid, are the same as Shibuya et al. (2015); the model top is 53 km and the number of the vertical level is 243 (Δz = 150 m up to 20 km). Simulations were performed for the time period from 0000 UTC 7 April to 0000 UTC 9 April 2013. As discussed in Shibuya et al. (2015), packets of gravity waves were distributed both over the Antarctic continent and the Southern Ocean in this period, which is consistent with the observation.

Geophysical locations and phase structures of gravity waves are quite similar between the two simulations (Supplement). Thus, we compare simulated momentum fluxes $\overline{u'w'}$ at the same geographical locations using these results in the period from 0000 UTC 8 April to 0000 UTC 9 April 2013. The fluctuations are extracted by a high-pass filter with a cutoff wavelength of 1000 km. Figure 5 shows a histogram of the ratio of the simulated momentum fluxes using the grid system by our transformation, $\overline{u'w'}$, to those using the grid system by Tomita et al. (2008), $\overline{u'w'}_{\text{Tomita}}$, as a function of latitude. The scatter plot in Fig. 5 is the ratio of the grid intervals of Tomita et al. (2008), d_{Tomita}, to those of our transformation, d. In the high-latitude region ($\phi < -60°$), the momentum fluxes using the grid system by Tomita et al. (2008) are larger than by our transformation, and vice versa in the mid-latitude region ($\phi > -60°$). Their features are consistent with the inverse ratio of the grid intervals (d_{Tomita}/d, as discussed in the previous studies (e.g., Plougonven et al., 2013). It should be noted that the center of the histogram of the ratio $\overline{u'w'}/\overline{u'w'}_{\text{Tomita}}$ approaches 1 at 60° S, where d_{Tomita} is just the same as d. Thus, the momentum flux simulated using the grid system by Tomita et al. (2008) seems to be numerically over-(under-)estimated in the high-(mid-)latitude region, compared with using the grid system by our transformation. This fact suggests that our transformation is quite useful for the estimation of the

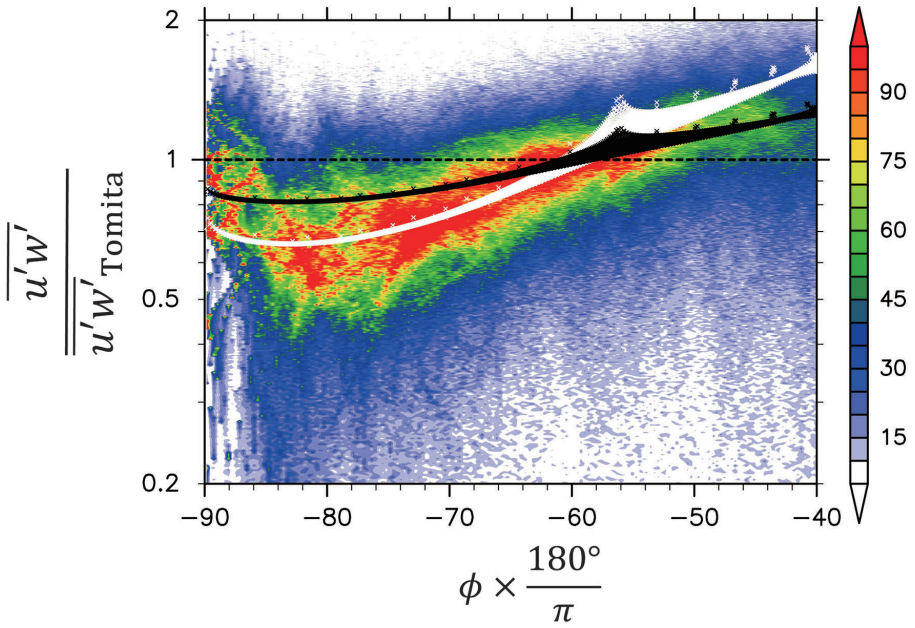

Fig. 5. A histogram of the ratio of the simulated momentum fluxes using the grid system by our transformation to those using the grid system by Tomita et al. (2008) ($\overline{u'w'}/\overline{u'w'}_{\mathrm{Tomita}}$) (as a function of latitude. The scatter plot (black cross marks) shows the ratio of the grid intervals of Tomita et al. (2008) to of our transformation (d_{Tomita}/d), while the scatter plot (white cross marks) shows $(d_{\mathrm{Tomita}}/d)^2$.

momentum fluxes in the target region.

Interestingly, the dependence of the momentum flux on the grid interval is stronger in the high-latitude region than in the mid-latitude region. The dependence at the high-latitude region roughly corresponds to $(d_{\mathrm{Tomita}}/d)^2$, which is also stronger than that reported by the previous studies (e.g., Plougonven et al. 2013). Further studies are needed to examine such a quantitative dependence of the momentum flux on the grid interval.

5. Summary and concluding remarks

We have proposed a new grid transformation with a finer and quasi-homogeneous grid in a target region using the spring dynamics. First, we formulated the constraint regarding the cell areas and the grid number in the variable-resolution system. We chose the Schmidt transformation as a latitudinal function of the resolution outside the target region to make the grid shapes as isotropic as possible. Second, a constraint regarding the area of the target region, the grid number in the target region, and the parameter of the Schmidt transformation was derived. As a result, it was shown that only one parameter that stands for the area of the target region is needed in our transformation, provided that the condition that the grid resolution in the target region is as fine as possible.

Our proposed transformation generates quasi-homogeneous grids in the target region. We compared our grid systems with those from the transformation in Tomita (2008). Our transformation yields comparable grid properties to that in Tomita (2008) in terms of the smoothness and the isotropy although the grid shapes are rather distorted near the edge latitude. Simulations using both transformations under a realistic atmospheric condition show the amplitudes of the momentum flux of gravity waves are strongly dependent on the grid intervals, suggesting that our transformation is quite useful for the estimation of the momentum fluxes.

It should be noted that this transformation can be applied to other grid systems using spring dynamics. These characteristics are important in terms of simulations of waves and mixing processes, the behaviors of which strongly depend on the resolution of the numerical model. Moreover, unlike regional models, this stretched grid model does not have the problem of artificial wave reflection at the domain boundaries.

Supplements

Supplementary Fig. S1 shows snapshots of horizontal maps of vertical gradient of vertical wind components at z = 15.0 km at (a) 1200 UTC 8 April 2013 using the grid systems generated (a) by Tomita (2008) and (b) by our transformation.

Acknowledgments

The authors thank the editor, Takeshi Horinouchi, and two anonymous reviewers for their critical reading and constructive comments which greatly improved the original manuscript. Numerical simulations were run on the supercomputer at NIPR and The University of Tokyo. All figures in this paper are pictured by using Dennou Club Library (DCL). This work was supported by the program for Leading Graduate Schools, MEXT, Japan. This study was also supported by Grant-in-Aid Scientific Research (A) 25247075 and by Grant-in-Aid for Research Fellow (26-9257) provided by the Japan Society for the Promotion of Science (JSPS).

References

Aghedo, A. M., S. Rast, and M. G. Schultz, 2010: Sensitivity of tracer transport to model resolution, prescribed meteorology and tracer lifetime in the general circulation model ECHAM5. *Atmos. Chem. Phys.*, **10**, 3385–3396.

Heikes, R., and D. A. Randall, 1995: Numerical integration of the shallow-water equations on a twisted icosahedral grid. Part I: Basic design and results of tests. *Mon. Wea. Rev.*, **123**, 1862–1880.

Iga, S., 2015: Smooth, seamless, and structured grid generation with flexibility in resolution distribution on a sphere based on conformal mapping and the spring dynamics method. *J. Comput. Phys.*, **297**, 381–406.

Miura, H., and M. Kimoto, 2005: A comparison of grid quality of optimized spherical hexagonal-pentagonal geodesic grids. *Mon. Wea. Rev.*, **133**, 2817–2833.

Miyakawa, T., M. Satoh, H. Miura, H. Tomita, H. Yashiro, A. T. Noda, Y. Yamada, C. Kodama, M. Kimoto, and K. Yoneyama, 2014: Madden-Julian Oscillation prediction skill of a new-generation global model. *Nat. Commun.*, **5**, 3769, doi:10.1038/ncomms4769.

Nasuno, T., 2013: Forecast skill of Madden-Julian Oscillation events in a global nonhydrostatic model during the CINDY2011/DYNAMO observation period. *SOLA*, **9**, 69–73.

Plougonven, R., A. Hertzog, and L. Guez, 2013: Gravity waves over Antarctica and the Southern Ocean: Consistent momentum fluxes in mesoscale simulations and stratospheric balloon observations. *Quart. J. Roy. Meteor. Soc.*, **139**, 101–118.

Sadourny, R., A. Arakawa, and Y. Mintz, 1968: Integration of the nondivergent barotropic vorticity equation with an icosahedral-hexiagonal grid for the sphere. *Mon. Wea. Rev.*, **96**, 351–356.

Satoh, M., T. Matsuno, H. Tomita, H. Miura, T. Nasuno, and S. Iga, 2008: Nonhydrostatic icosahedral atmospheric model (NICAM) for global cloud resolving simulations. *J. Comput. Phys.*, **227**, 3486−3514.

Satoh, M., H. Tomita, H. Yashiro, H. Miura, C. Kodama, T. Seiki, A. T. Noda, Y. Yamada, D. Goto, M. Sawada, T. Miyoshi, Y. Niwa, M. Hara, T. Ohno, S. Iga, T. Arakawa, T. Inoue, and H. Kubokawa, 2014: The Non-hydrostatic Icosahedral Atmospheric Model: Description and development. *Prog. Earth Planet. Sci.*, **1**, 18, doi:10.1186/s40645-014-0018-1.

Shibuya, R., K. Sato, Y. Tomikawa, M. Tsutsumi, and T. Sato, 2015: A study of multiple tropopause structures caused by inertia-gravity waves in the Antarctica. *J. Atmos. Sci.*, **72**, 2109–2130.

Tomita, H., 2008: A stretched grid on a sphere by new grid transformation. *J. Meteor. Soc. Japan*, **86A**, 107–119.

Tomita, H., and M. Satoh, 2004: A new dynamical framework of nonhydrostatic global model using the icosahedral grid. *Fluid Dyn. Res.*, **34**, 357–400.

Tomita, H., M. Tsugawa, M. Satoh, and K. Goto, 2001: Shallow water model on a modified icosahedral geodesic grid by using spring dynamics. *J. Comput. Phys.*, **174**, 579–613.

Tomita, H., M. Satoh, and K. Goto, 2002: An optimization of icosahedral grid by using spring dynamics. *J. Comput. Phys.*, **183**, 307–331.

Williamson, D. L., 1968: Integration of the barotropic vorticity equation on a spherical geodesic grid. *Tellus*, **20**, 642−653.